Supplementary Information *for* **Generalization of elastohydrodynamic interactions between a rigid sphere and a nearby soft wall**

Pratyaksh Karan, Jeevanjyoti Chakraborty, Suman Chakraborty†

†Email address for correspondence: suman@mech.iitkgp.ac.in

S1 Transformation Procedure

1. *Transformation of Independent Variables*: We transform the independent variables using their characteristic scales. The scale for t^* is $\frac{1}{\omega}$, giving us $t = \omega t^*$. The scales for the other independent variables are dependent upon the geometry and imposed dynamics being considered, which are divided into two categories - $\alpha \ll 1$ and $\alpha \sim 1$. Here, we emphasize two points. First, the scale for $\bar{z}^*$ is taken as δR, giving us $\bar{z}^* = \delta R \bar{z}$, where the expression for δ is obtained out of considerations for the deformation characteristics, as presented in section 2.6. Second, the scale of r^* is the same in the fluid domain and the substrate domain, as the load on the substrate comes from the fluid domain.
   We first consider the case of $\alpha \ll 1$, i.e. the range of motion of the sphere is small compared to its mean separation from the origin. For this case, the scale for z^* is $D = \epsilon R$, giving us $z^* = \epsilon R z$. Subsequently, following the classical lubrication methodology (Urzay, 2010; Leal, 2007), the scale for r^* is $\sqrt{RD} = \epsilon^{\frac{1}{2}} R$, giving us $r^* = \epsilon^{\frac{1}{2}} R r$.
   Next, we consider the case of $\alpha \sim 1$, i.e. the sphere displacement over its range of motion is comparable to its mean separation from the origin. The prime consequence of $\alpha \sim 1$ is that the scale for z^* is,

$$z^* \sim d(t^*) = \left\{ \begin{array}{ll} D + h_0 \cos(\omega t^*) = (1 + \alpha \cos(\omega t^*))\epsilon R & \text{oscillatory,} \\ D + h_0(1 - \omega t^*) = (1 + \alpha(1 - \omega t^*))\epsilon R & \text{approach,} \\ D - h_0(1 - \omega t^*) = (1 - \alpha(1 - \omega t^*))\epsilon R & \text{recession,} \end{array} \right\} = k(t^*)\epsilon R,$$

   giving us $z^* = k(t^*)\epsilon R z$. Again, following the classical lubrication methodology, the scale for r^* is $\sqrt{Rd} = k(t^*)^{\frac{1}{2}} \epsilon^{\frac{1}{2}} R$, giving us $r^* = k(t^*)^{\frac{1}{2}} \epsilon^{\frac{1}{2}} R r$. We note that the expression for δ for this case can be time-dependent as well, i.e. $\delta = \delta(t^*)$ (see section 2.6).

2. *Transformation of Derivatives*: When we consider time-dependent scales for the independent spatial variables for the physical setup, as done in the case of $\alpha \sim 1$ above, it is equivalent to performing a transformation of the system domains such that the z^* in the original system scales to a unity-scaled z in the mapped system. The consequence of this mapping is the transformation, in the governing equation and boundary conditions, of independent variables as per the expressions presented in the last step (as well as in table 1), and in derivative terms as per transformation template we will derive ahead.
   In table S1, under the column 'forward', we present how the independent variables in the mapped co-ordinate system $(r, z, \bar{z}, t)$ are expressed in terms of the independent variables in the original coordinate system $(r^*, z^*, \bar{z}^*, t^*)$. Under the column 'backward (partial)', we present how the independent variables in the original coordinate system are expressed in terms of the independent variables in the mapped coordinate system. These expressions are obtained simply by doing trivial algebra on the expressions for the independent variables in the mapped coordinate system in terms of the independent variables in the original co-ordinate system.
   Examining the expressions in the column 'backward (partial)', we can see that the independent variables in original coordinate system are not expressed exclusively in terms of the independent variables in the mapped coordinate system, due to the presence of functions of t^*, $k(t^*)$ and $\delta(t^*)$. To remedy this, we take the help of the last row in the table S1 and observe that a general function of t^* in the original coordinate system

Table S1: Forward and Backward Mapping from $(r^*, z^*, \bar{z}^*, t^*)$ to $(r, z, \bar{z}, t)$

forward	**backward (partial)**	**backward**
$r = \dfrac{r^*}{k(t^*)^{\frac{1}{2}}\epsilon^{\frac{1}{2}}R}$	$r^* = k(t^*)^{\frac{1}{2}}\epsilon^{\frac{1}{2}}Rr$	$r^* = k(t)^{\frac{1}{2}}\epsilon^{\frac{1}{2}}Rr$
$z = \dfrac{z^*}{k(t^*)\epsilon R}$	$z^* = k(t^*)\epsilon Rz$	$z^* = k(t)\epsilon Rz$
$\bar{z} = \dfrac{\bar{z}^*}{\delta(t^*)R}$	$\bar{z}^* = \delta(t^*)Rz$	$\bar{z}^* = \delta(t)Rz$
$t = \omega t^*$	$t^* = \dfrac{t}{\omega}$	$t^* = \dfrac{t}{\omega}$

transforms to a general function of t in the mapped co-ordinate system,

$$f(t^*) \equiv f(t^*(t)) = f(t) \tag{S1}$$

This gives us the transformations: $k(t^*) \equiv k(t)$ and $\delta(t^*) \equiv \delta(t)$. Substituting these in the column 'backward (partial)' gives us the column 'backward'. Together, columns 'forward' and 'backward' represent the bijective mapping between the two co-ordinate systems.
Based on this obtained mapping, functions of various combinations of independent variables in original coordinate system undergo functional transformations as,

$$f(t^*) \equiv f(t^*(t)) = f(t) \tag{S2a}$$

$$f(r^*, t^*) \equiv f(r^*(r,t), t^*(t)) = f(r,t) \tag{S2b}$$

$$f(r^*, z^*, t^*) \equiv f(r^*(r,t), z^*(z,t), t^*(t)) = f(r,z,t) \tag{S2c}$$

$$f(r^*, \bar{z}^*, t^*) \equiv f(r^*(r,t), \bar{z}^*(\bar{z},t), t^*(t)) = f(r,\bar{z},t) \tag{S2d}$$

Knowing this functional transformation, we will obtain expressions for the pertinent derivatives in the original coordinate systems in terms of the derivatives in the mapped coordinate system. The general expression for this transformation, using the chain rule, is,

$$\frac{\partial \mathbb{U}}{\partial \mathbb{X}^*} \equiv \frac{\partial \mathbb{U}}{\partial r}\frac{\partial r}{\partial \mathbb{X}^*} + \frac{\partial \mathbb{U}}{\partial z}\frac{\partial z}{\partial \mathbb{X}^*} + \frac{\partial \mathbb{U}}{\partial \bar{z}}\frac{\partial \bar{z}}{\partial \mathbb{X}^*} + \frac{\partial \mathbb{U}}{\partial t}\frac{\partial t}{\partial \mathbb{X}^*}, \tag{S3}$$

where $\mathbb{U}$ is a general dependent variable and $\mathbb{X}^*$ is a general independent variables. The second order derivatives are obtained recursively by plugging $\dfrac{\partial \mathbb{U}}{\partial \mathbb{X}^*}$ in place of $\mathbb{U}$ in equation (S3).
As evident from equation (S3), in order to proceed further, we have to evaluate some derivatives of the independent variables in the mapped co-ordinate system with respect to the independent variables in the original co-ordinate system. These are,

$$\frac{\partial t}{\partial t^*} = \frac{\partial(\omega t^*)}{\partial t^*} = \omega, \tag{S4a}$$

$$\frac{\partial r}{\partial t^*} = \frac{\partial}{\partial t^*}\left(\frac{r^*}{k(t^*)^{\frac{1}{2}}\epsilon^{\frac{1}{2}}R}\right) = -\frac{r^*}{2k^{\frac{3}{2}}\epsilon^{\frac{1}{2}}R}\frac{dk}{dt^*} = -\frac{r}{2k}\frac{dh}{dt^*} \equiv -\frac{\omega r}{2k}\frac{dk}{dt}, \tag{S4b}$$

$$\frac{\partial z}{\partial t^*} \equiv -\frac{\omega z}{k}\frac{dk}{dt}, \qquad \frac{\partial \bar{z}}{\partial t^*} \equiv -\frac{\omega \bar{z}}{\delta}\frac{d\delta}{dt}, \tag{S4c}$$

$$\frac{\partial r}{\partial r^*} \equiv \frac{1}{k^{\frac{1}{2}}\epsilon^{\frac{1}{2}}R}, \qquad \frac{\partial z}{\partial z^*} \equiv \frac{1}{k\epsilon R}, \qquad \frac{\partial \bar{z}}{\partial \bar{z}^*} \equiv \frac{1}{\delta R}. \tag{S4d}$$

All other combinations, that are not presented in equation (S4), are zero. Equation (S4a) is straightforward to derive. In equation (S4b), the second last step involves substituting the expression for r^* in terms of r (from 'backward' column of table S1), and the last step (i.e. the '$\equiv$' step) involves transforming $\dfrac{dk}{dt^*}$ to $\dfrac{dk}{dt}$ using equation (S3). Since k is a function of only t, the first three terms (i.e. $\dfrac{\partial k}{\partial r}$, $\dfrac{\partial k}{\partial z}$, and $\dfrac{\partial k}{\partial \bar{z}}$) vanish, and substituting $\dfrac{\partial t}{\partial t^*} = \omega$ from equation (S4a) gives $\dfrac{dk}{dt^*} \equiv \omega\dfrac{dk}{dt}$. Equations (S4c) and (S4d) are obtained using

similar procedure as for equation (S4b).
Using equations (S3) and (S4), the transformation template for the derivatives is obtained as,

$$\frac{\partial \mathbb{U}}{\partial t^*} \equiv \omega \left[\frac{\partial \mathbb{U}}{\partial t} - \left\{ \left(\frac{r}{2} \frac{\partial \mathbb{U}}{\partial r} + z \frac{\partial \mathbb{U}}{\partial z} \right) \frac{1}{k} \frac{dk}{dt} + \frac{\bar{z}}{\delta} \frac{d\delta}{dt} \frac{\partial \mathbb{U}}{\partial \bar{z}} \right\} \right], \tag{S5a}$$

$$\frac{\partial \mathbb{U}}{\partial r^*} \equiv \frac{1}{k^{\frac{1}{2}} \epsilon^{\frac{1}{2}} R} \frac{\partial \mathbb{U}}{\partial r}, \quad \frac{\partial^2 \mathbb{U}}{\partial r^{*2}} \equiv \frac{1}{k \epsilon R^2} \frac{\partial^2 \mathbb{U}}{\partial r^2}, \tag{S5b}$$

$$\frac{\partial \mathbb{U}}{\partial z^*} \equiv \frac{1}{k \epsilon R} \frac{\partial \mathbb{U}}{\partial z}, \quad \frac{\partial^2 \mathbb{U}}{\partial z^{*2}} \equiv \frac{1}{k^2 \epsilon^2 R^2} \frac{\partial^2 \mathbb{U}}{\partial z^2}, \tag{S5c}$$

$$\frac{\partial \mathbb{U}}{\partial \bar{z}^*} \equiv \frac{1}{\delta R} \frac{\partial \mathbb{U}}{\partial \bar{z}}, \quad \frac{\partial^2 \mathbb{U}}{\partial \bar{z}^{*2}} \equiv \frac{1}{\delta^2 R^2} \frac{\partial^2 \mathbb{U}}{\partial \bar{z}^2}, \tag{S5d}$$

3. *Transformation of Dependent Variables*:

The scale for substrate displacement, $\vec{u}^*$ is taken as θR, giving us $\vec{u}^* = \theta R \vec{u}$. The expressions for θ and θ_{S} depend on the applied load, and are obtained in section 2.6. The scale for the net effective pressure, p^*, is taken as Π, whose expression is dependent on the force interactions in the system, and is also obtained in section 2.6. The scale for l^* is the same as the scale for $\vec{u}^*$, giving us $l^* = \theta R l$. H_{I}^* and H_{S}^* are scaled similar to z^*, giving us $H_{\mathrm{I}}^* = \epsilon R H_{\mathrm{I}}$ and $H_{\mathrm{S}}^* = \epsilon R H_{\mathrm{S}}$. Lastly, we scale l_{S}^* with $\theta_{\mathrm{S}} R$, such that $l_{\mathrm{S}}^* = \theta_{\mathrm{S}} R l_{\mathrm{S}}$.
Collating the expressions for the two cases of $\alpha \ll 1$ and $\alpha \sim 1$, we find that they can be collectively represented as $z^* = k\epsilon R z$, $r^* = k^{\frac{1}{2}} \epsilon^{\frac{1}{2}} R r$, $v_r^* = \dfrac{\epsilon^{\frac{1}{2}} \alpha \omega R}{k^{\frac{1}{2}}} v_r$, $v_z^* = \epsilon \alpha \omega R v_z$, $p_{\mathrm{hd}}^* = \dfrac{\mu \omega \alpha}{k^2 \epsilon} p_{\mathrm{hd}}$, and $H^* = k\epsilon R H$, with the expressions for k and H as presented in equations (2.24a) and (2.24b).

S2 Transformed Governing Equation and Boundary Conditions

All the governing equations and boundary conditions (in section 2.2) are transformed as per the transformation detailed in sections 2.4 and S1. These equations are listed ahead.

- Continuity equation (from equation (2.4)):

$$\frac{1}{r} \frac{\partial (r v_r)}{\partial r} + \frac{\partial v_z}{\partial z} = 0 \tag{S6}$$

- Momentum-conservation equation (or the Navier-Stokes equation, from equation (2.5)):

$$\frac{k\epsilon^2 \rho \omega R^2}{\mu} \left[k \frac{\partial v_r}{\partial t} - \frac{v_r}{2} \frac{dk}{dt} - \frac{1}{2} \frac{dk}{dt} \left(r \frac{\partial v_r}{\partial r} + 2z \frac{\partial v_r}{\partial z} \right) + \alpha \left(v_r \frac{\partial v_r}{\partial r} + v_z \frac{\partial v_r}{\partial z} \right) \right] = - \frac{\partial p_{\mathrm{hd}}}{\partial r} + \frac{\partial^2 v_r}{\partial z^2} + k\epsilon \left[\frac{1}{r} \frac{\partial}{\partial r} \left(r \frac{\partial v_r}{\partial r} \right) - \frac{v_r}{r^2} \right] \tag{S7a}$$

$$\frac{k^2 \epsilon^3 \rho \omega R^2}{\mu} \left[k \frac{\partial v_z}{\partial t} - \frac{1}{2} \frac{dk}{dt} \left(r \frac{\partial v_z}{\partial r} + 2z \frac{\partial v_z}{\partial z} \right) + \alpha \left(v_r \frac{\partial v_z}{\partial r} + v_z \frac{\partial v_z}{\partial z} \right) \right] = - \frac{\partial p_{\mathrm{hd}}}{\partial z} + k\epsilon \frac{\partial^2 v_r}{\partial z^2} + k^2 \epsilon^2 \left[\frac{1}{r} \frac{\partial}{\partial r} \left(r \frac{\partial v_z}{\partial r} \right) \right] \tag{S7b}$$

- No-slip and no-penetration conditions at the fluid-sphere interface, i.e. at $z = H = H_{\mathrm{I}} + \Gamma_{\mathrm{S}} l_{\mathrm{S}}$ (from equation (2.6)):

$$v_r = 0 \tag{S8a}$$

$$v_z = V_{\mathrm{I}} + V_{\mathrm{S}} \tag{S8b}$$

where,

$$V_{\mathrm{I}} = \begin{cases} -\sin(t) & \text{oscillatory} \\ -1 & \text{approach} \\ 1 & \text{recession} \end{cases} \tag{S9a}$$

$$V_{\mathrm{S}} = \frac{\Gamma_{\mathrm{S}}}{\alpha} \left[k \frac{\partial l_{\mathrm{S}}}{\partial t} + \frac{k l_{\mathrm{S}}}{\theta_{\mathrm{S}}} \frac{d\theta_{\mathrm{S}}}{dt} \right] \tag{S9b}$$

- No slip and no penetration conditions at the fluid-substrate interface, i.e. at $z = -\Gamma l$ (from equation (2.8)):

$$v_r = 0, \tag{S10a}$$

$$v_z = -\frac{\Gamma}{\alpha}\left[k\frac{\partial l}{\partial t} + \frac{kl}{\theta}\frac{d\theta}{dt} - \frac{r}{2}\frac{dk}{dt}\frac{\partial l}{\partial r}\right] = -V_{\mathrm{C}} \tag{S10b}$$

- Zero velocity and zero hydrodynamic pressure conditions at far-end of the lubrication zone, i.e. as $r \to \infty$ (from equation (2.9)):

$$v_r \to 0,\ v_z \to 0,\ p_{\mathrm{hd}} \to 0 \tag{S11}$$

- Zero radial velocity and symmetric axial velocity and hydrodynamic pressure conditions at the centerline, i.e. at $r = 0$ (from equation (2.10)):

$$v_r = \frac{\partial v_z}{\partial r} = \frac{\partial p_{\mathrm{hd}}}{\partial r} = 0 \tag{S12}$$

- Mechanical equilibrium equation (from equation (2.13)):

$$\frac{\partial^2 u_r}{\partial \bar{z}^2} + \frac{\delta}{k^{\frac{1}{2}}\epsilon^{\frac{1}{2}}}\left(1 + \frac{\lambda}{G}\right)\frac{\partial^2 u_{\bar{z}}}{\partial r \partial \bar{z}} + \frac{\delta^2}{k\epsilon}\left(2 + \frac{\lambda}{G}\right)\left(\frac{\partial^2 u_r}{\partial r^2} + \frac{1}{r}\frac{\partial u_r}{\partial r} - \frac{u_r}{r^2}\right) = 0 \tag{S13a}$$

$$\left(2 + \frac{\lambda}{G}\right)\frac{\partial^2 u_{\bar{z}}}{\partial \bar{z}^2} + \frac{\delta}{k^{\frac{1}{2}}\epsilon^{\frac{1}{2}}}\left(1 + \frac{\lambda}{G}\right)\left(\frac{\partial^2 u_r}{\partial r \partial \bar{z}} + \frac{1}{r}\frac{\partial u_r}{\partial \bar{z}}\right) + \frac{\delta^2}{k\epsilon}\left(\frac{\partial^2 u_{\bar{z}}}{\partial r^2} + \frac{1}{r}\frac{\partial u_{\bar{z}}}{\partial r}\right) = 0 \tag{S13b}$$

- Zero-displacement condition at far-end of the lubrication zone, i.e. as $r \to \infty$ (from equation (2.14)):

$$u_r \to 0,\ u_{\bar{z}} \to 0 \tag{S14}$$

- Zero-displacement condition at substrate-platform interface, i.e. at $\bar{z}^* = L$ or $\bar{z} = \dfrac{\beta}{\delta}$ (from equation (2.15)):

$$u_r = u_{\bar{z}} = 0 \tag{S15}$$

- Zero radial displacement and symmetric axial displacement at the centerline, i.e. at $r = 0$ (from equation (2.16)):

$$u_r = \frac{\partial u_{\bar{z}}}{\partial r} = 0 \tag{S16}$$

- Traction balance condition at fluid-substrate interface, i.e. at $\bar{z} = 0$ (from equation (2.19)):

$$\frac{\partial u_r}{\partial \bar{z}} + \frac{\delta}{k^{\frac{1}{2}}\epsilon^{\frac{1}{2}}}\frac{\partial u_{\bar{z}}}{\partial r} = \frac{\delta\Pi}{\theta(\lambda + 2G)} \cdot \left\{\left(2 + \frac{\lambda}{G}\right)\left(\frac{1}{k^2}\frac{\mu\omega\alpha}{\epsilon\Pi}\right)\left(k^{\frac{1}{2}}\epsilon^{\frac{1}{2}}\left(\frac{\partial v_r}{\partial z} + k\epsilon\frac{\partial v_z}{\partial r}\right)\right)\right\} \tag{S17a}$$

$$\frac{\partial u_{\bar{z}}}{\partial \bar{z}} + \frac{\delta}{k^{\frac{1}{2}}\epsilon^{\frac{1}{2}}}\left(\frac{\lambda}{\lambda + 2G}\right)\left(\frac{\partial u_r}{\partial r} + \frac{u_r}{r}\right) = -\frac{\delta\Pi}{\theta(\lambda + 2G)} \cdot \left[p - \left\{\left(\frac{1}{k^2}\frac{\mu\omega\alpha}{\epsilon\Pi}\right)\left(2k\epsilon\frac{\partial v_z}{\partial z}\right)\right\}\right] \tag{S17b}$$

S3 Hankel-Space Deflection-Pressure Relation

We consider the Airy stress function, Φ, defined as,

$$\begin{aligned} u_r &= -\frac{\delta}{k^{\frac{1}{2}}\epsilon^{\frac{1}{2}}}\left(1 + \frac{\lambda}{G}\right)\frac{\partial^2 \Phi}{\partial r \partial \bar{z}}, \\ u_{\bar{z}} &= \frac{\partial^2 \Phi}{\partial \bar{z}^2} + \frac{\delta^2}{k\epsilon}\frac{1}{r}\frac{\partial}{\partial r}\left(r\frac{\partial \Phi}{\partial r}\right). \end{aligned} \tag{S18}$$

Substituting these expressions in equation (S13), the first sub-equation gets trivially satisfied and the second one converts into the non-dimensional biharmonic equation,

$$\mathrm{B}\Phi = 0, \tag{S19}$$

where, B is the non-dimensional biharmonic operator,

$$\mathrm{B} = \mathrm{L}^2 = \left[\frac{\partial^2}{\partial \bar{z}^2} + \frac{\delta^2}{\epsilon}\left(\frac{\partial^2}{\partial r^2} + \frac{1}{r}\frac{\partial}{\partial r}\right)\right]^2, \tag{S20}$$

Following an analogous approach to that applied by Harding & Sneddon (1945) for the dimensional version of equation (S20), we obtain the governing equation for the zero-eth order Hankel transform of Φ, $\tilde{\Phi}$, as,

$$\left(\frac{\partial^2}{\partial \bar{z}^2} - \chi^2\right)\tilde{\Phi} = 0, \tag{S21}$$

where χ is $\dfrac{\delta x}{k^{\frac{1}{2}}\epsilon^{\frac{1}{2}}}$, x is the Hankel-space counterpart of r, the n-th order Hankel transform of an arbitrary function of r, $\mathbb{V}(r)$, is given as,

$$H_n[\mathbb{V}(r)] = \int_0^\infty dr \cdot rJ_n(xr) \cdot \mathbb{V}(r), \tag{S22}$$

and the presence of an accent $\tilde{}$ (e.g. in $\tilde{\mathbb{V}}(x)$) denotes that the Hankel transform is zero-eth order, i.e. $\tilde{\mathbb{V}}(x) = H_0[\mathbb{V}(r)]$.

Equation (S21) admits the solution of the form,

$$\tilde{\Phi} = (\mathbb{A} + \mathbb{B}y)\exp(\chi z) + (\mathbb{C} + \mathbb{D}y)\exp(-\chi z). \tag{S23}$$

The constants of integration, $\mathbb{A}$ to $\mathbb{D}$, are obtained from the boundary conditions. This equation, whose foundation was laid by Harding & Sneddon (1945) and Muki (1960), has been used to solve multiple problems of axisymmetric as well as general deformation field in setups ranging from coatings to semi-infinite media to stratified soft layers to continuously graded solid domains (Dhaliwal & Rau, 1970; Chan *et al.*, 1974; Giannakopoulos & Suresh, 1997; Li & Chou, 1997; Selvadurai & Lan, 1998; Yang, 1998; Ai *et al.*, 2002; Yang, 2003; Gacoin *et al.*, 2006; Zhao & Rajapakse, 2009; Selvadurai, 2009; Leroy & Charlaix, 2011; Wang *et al.*, 2017). For the substrate-coating of arbitrary thickness undergoing axisymmetric loading that we are studying, equations (S14) and (S16) get trivially satisfied, and equations (S15) and (S17) provide the values of $\mathbb{A}$ to $\mathbb{D}$.
Plugging in the expression for θ and retaining only the leading order terms, equation (S17) simplifies to,

$$\frac{\partial u_r}{\partial y} + \frac{\delta}{k^{\frac{1}{2}}\epsilon^{\frac{1}{2}}}\frac{\partial u_y}{\partial r} = 0 \tag{S24a}$$

$$\frac{\partial u_y}{\partial y} + \frac{\delta}{k^{\frac{1}{2}}\epsilon^{\frac{1}{2}}}\left(\frac{\lambda}{\lambda + 2G}\right)\left(\frac{\partial u_r}{\partial r} + \frac{u_r}{r}\right) = -p \tag{S24b}$$

These simplified equations are equivalent to the condition of $\sigma_{(S)ry} = 0, \sigma_{(S)yy} = q$ at the substrate domain boundary with distributed load q, that was applied by Harding & Sneddon (1945); Li & Chou (1997). Hence following algebra

similar to theirs and employing equation (S24) and equation (S15), the expressions for $\mathbb{A}$ to $\mathbb{D}$ are obtained as,

$$\begin{aligned}
\mathbb{A} =& \frac{b\epsilon^{\frac{3}{2}}\Pi}{k^{\frac{3}{2}}\delta^2\theta}\frac{\tilde{p}}{2x^3}\exp\left(-\gamma x\right)\cdot \\
& \left[\frac{\left\{(\lambda+G)^3(2\gamma^2+1)+2\lambda(\lambda+G)\gamma x+G(\lambda+3G)\right\}\exp(\gamma x)+\lambda(\lambda+3G)\exp(-\gamma x)}{2(\lambda+G)^3(2\gamma^2+1)+4G(\lambda+G)(\lambda+2G)+(\lambda+G)^2(\lambda+3G)\left\{\exp(2\gamma x)+\exp(-2\gamma x)\right\}}\right], \\
\mathbb{B} =& -\frac{b\epsilon^{\frac{3}{2}}\Pi}{k^{\frac{3}{2}}\delta^2\theta}\frac{\tilde{p}}{2x^3}\exp\left(-\gamma x\right)\cdot \\
& \left[\frac{(\lambda+G)(2\gamma x+1)\exp(\gamma x)+(\lambda+3G)\exp(-\gamma x)}{2(\lambda+G)^3(2\gamma^2+1)+4G(\lambda+G)(\lambda+2G)+(\lambda+G)^2(\lambda+3G)\left\{\exp(2\gamma x)+\exp(-2\gamma x)\right\}}\right], \\
\mathbb{C} =& -\frac{b\epsilon^{\frac{3}{2}}\Pi}{k^{\frac{3}{2}}\delta^2\theta}\frac{\tilde{p}}{2x^3}\exp\left(-\gamma x\right)\cdot \\
& \left[\frac{\left\{(\lambda+G)^3(2\gamma^2+1)-2\lambda(\lambda+G)\gamma x+G(\lambda+3G)\right\}\exp(-\gamma x)+\lambda(\lambda+3G)\exp(\gamma x)}{2(\lambda+G)^3(2\gamma^2+1)+4G(\lambda+G)(\lambda+2G)+(\lambda+G)^2(\lambda+3G)\left\{\exp(2\gamma x)+\exp(-2\gamma x)\right\}}\right], \\
\mathbb{D} =& \frac{b\epsilon^{\frac{3}{2}}\Pi}{k^{\frac{3}{2}}\delta^2\theta}\frac{\tilde{p}}{2x^3}\exp\left(-\gamma x\right)\cdot \\
& \left[\frac{(\lambda+G)(2\gamma x-1)\exp(-\gamma x)-(\lambda+3G)\exp(\gamma x)}{2(\lambda+G)^3(2\gamma^2+1)+4G(\lambda+G)(\lambda+2G)+(\lambda+G)^2(\lambda+3G)\left\{\exp(2\gamma x)+\exp(-2\gamma x)\right\}}\right],
\end{aligned} \tag{S25}$$

where $\gamma = \dfrac{\beta}{k^{\frac{1}{2}}\epsilon^{\frac{1}{2}}}$ and $\tilde{p}$ is the zero-eth order Hankel transform of pressure p.
The first-order Hankel transform of u_r, $H_1[u_r]$, and the zeroeth-order Hankel transform of $u_{\bar{z}}$, $\tilde{u}_{\bar{z}}$, in terms of $\tilde{\Phi}$ and its derivatives with $\bar{z}$ are,

$$\begin{aligned}
H_1[u_r] &= -\frac{\delta x}{k^{\frac{1}{2}}\epsilon^{\frac{1}{2}}}\frac{\partial\tilde{\Phi}}{\partial\bar{z}} \\
\tilde{u}_{\bar{z}} &= \frac{\partial^2\tilde{\Phi}}{\partial\bar{z}^2}-\left(2+\frac{\lambda}{G}\right)\frac{\delta^2x^2}{k\epsilon}\frac{\partial\tilde{\Phi}}{\partial\bar{z}}
\end{aligned} \tag{S26}$$

The expression for the zero-eth order Hankel transform of deflection l, $\tilde{l}$, is obtained by taking the expression for $\tilde{u}_{\bar{z}}$ at $\bar{z}=0$, giving us equation (2.34). For the special case of incompressible substrate material, considering the alternate expression for θ as presented in section 2.6 leads to equation (S24b) changing to,

$$\frac{\partial u_y}{\partial y}+\frac{\delta}{k^{\frac{1}{2}}\epsilon^{\frac{1}{2}}}\left(\frac{\lambda}{\lambda+2G}\right)\left(\frac{\partial u_r}{\partial r}+\frac{u_r}{r}\right)=-\left(\frac{\lambda_{\mathrm{C}}+2G}{\lambda+2G}\right)p, \tag{S27}$$

with corresponding changes in the expressions for $\mathbb{A}$ to $\mathbb{D}$, such that we obtain the expression for X as presented in equation (2.36).

S4 Thickness and Compressibility Limits

The expression for X as given in equation (2.35) is a generic expression applicable for any substrate thickness and Poisson's ratio. However, its approximate expressions for various limiting cases provide us with some insights.
For the limiting case of thin substrate, $\delta \ll k^{\frac{1}{2}}\epsilon^{\frac{1}{2}}$ and therefore $\delta=\beta$ and $\gamma \ll 1$. This implies,

$$\begin{aligned}
\exp(-4\gamma x) &\approx 1-4\gamma x+8\gamma^2x^2-\frac{32}{3}\gamma^3x^3+O(\gamma^4x^4), \\
\exp(-2\gamma x) &\approx 1-2\gamma x+2\gamma^2x^2-\frac{4}{3}\gamma^3x^3+O(\gamma^4x^4).
\end{aligned} \tag{S28}$$

Substituting these approximations in equation (2.35) or (2.36) (as applicable) and keeping only the respectively highest ordered terms in the numerator and the denominator, the approximate expression for X is,

$$X=\begin{cases} 1 & 0\le\nu<0.5 \\ -\dfrac{\gamma^2}{3}\left(\dfrac{\lambda_{\mathrm{C}}+2G}{G}\right)x^2, & \nu=0.5 \end{cases} \tag{S29}$$

Substituting these expressions in equation (2.34) gives,

$$\tilde{l} = \begin{cases} \dfrac{\beta\tilde{p}}{\delta} & 0 \le \nu < 0.5 \\ -\dfrac{\beta}{\delta}\dfrac{\gamma^2}{3}\left(\dfrac{\lambda_{\mathrm{C}}+2G}{G}\right)x^2\tilde{p}, & \nu = 0.5 \end{cases} \tag{S30}$$

This equation can be straightaway inverted to give,

$$l = \begin{cases} \dfrac{\beta p}{\delta} & 0 \le \nu < 0.5 \\ -\dfrac{\beta}{\delta}\dfrac{\gamma^2}{3}\left(\dfrac{\lambda_{\mathrm{C}}+2G}{G}\right)\dfrac{\partial^2 p}{\partial r^2}, & \nu = 0.5 \end{cases} \implies l^* = \begin{cases} \dfrac{Lp^*}{\lambda+2G} & 0 \le \nu < 0.5 \\ -\dfrac{L^3}{3G}\dfrac{\partial^2 p^*}{\partial r^{*2}}, & \nu = 0.5 \end{cases} \tag{S31}$$

The deflection-pressure relation in equation (S31) matches those obtained in other EHD and soft-lubrication studies involving thin soft coatings, for the compressible case (Skotheim & Mahadevan, 2004) and in the incompressible limit (Chandler & Vella, 2020).

On the other hand, for the limiting case of a semi-infinite substrate, $\delta = k^{\frac{1}{2}}\epsilon^{\frac{1}{2}}$ and $\gamma \gg 1$, implying,

$$\gamma x \gg \gamma^3 x^3 \exp\left(-2\gamma x\right) \gg \gamma x \exp\left(-2\gamma x\right) \gg \gamma x \exp\left(-4\gamma x\right) \gg \exp\left(-4\gamma x\right). \tag{S32}$$

Substituting these approximations in equation (2.35) or (2.36) (as applicable) and keeping only the respectively highest ordered terms in the numerator and the denominator, the approximate expression for X is,

$$X = \begin{cases} \dfrac{(\lambda+2G)^2}{2G(\lambda+G)\gamma x} & 0 \le \nu < 0.5 \\ \dfrac{(\lambda+2G)(\lambda_{\mathrm{C}}+2G)}{2G(\lambda+G)\gamma x} = \dfrac{(\lambda_{\mathrm{C}}+2G)}{2G\gamma x}, & \nu = 0.5 \end{cases} \tag{S33}$$

Substituting these expressions in equation (2.34) gives,

$$\tilde{l} = \begin{cases} \dfrac{(\lambda+2G)^2}{2G(\lambda+G)}\dfrac{\tilde{p}}{x} & 0 \le \nu < 0.5 \\ \dfrac{(\lambda_{\mathrm{C}}+2G)}{2G}\dfrac{\tilde{p}}{x}, & \nu = 0.5 \end{cases} \tag{S34}$$

Evidently, equation (S34) cannot be inverted straightaway to get a real-space relation between pressure and deflection. The presence of x in the right hand side indicates that for a semi-infinite substrate, the deflection at each point (on the r-axis) is theoretically dependent on the pressure distribution along the complete radial span. This dependence exists for intermediate thicknesses a well, down until the substrate thickness reaches the thin-compressible limit (the top expressions in equations (S30) and (S31)), when the deflection at a radial point becomes solely dependent on the pressure at that radial point.

We next turn attention to substrate compressibility. The compressibility of any material is characterized by the Poisson's ratio. For most linear-elastic materials, Poisson's ratio has a value between 0 and 0.5, with the Poisson's ratio of 0.5 for incompressible materials. Materials with Poisson's ratio closer to 0.5 exhibit lower compressibility. We consider two limits of material compressibility, a 'perfectly incompressible limit (PIL)' having $\nu = 0.5$ and a corresponding opposite limit that we refer to as 'perfectly compressible limit (PCL)', for which $\nu = 0$. These limits correspond to $\lambda \to \infty$ and $\lambda = 0$ respectively, given that its expression is $\lambda = \dfrac{\nu E_{\mathrm{Y}}}{(1+\nu)(1-2\nu)} = \dfrac{2\nu G}{1-2\nu}$. On the other hand, G, whose expression in terms of E_{Y} and ν is $\dfrac{E_{\mathrm{Y}}}{2(1+\nu)}$, varies merely from $\dfrac{E_{\mathrm{Y}}}{3}$ to $\dfrac{E_{\mathrm{Y}}}{2}$ as ν varies from 0 to 0.5. Therefore, PCL corresponds to $\dfrac{\lambda}{G} = 0$ and PIL corresponds to $\dfrac{G}{\lambda} = 0$. The expressions for X in PIL are presented in equation (2.36), (S29) (bottom expression) and (S33) (bottom expression) for general thickness, thin limit and semi-infinite limit respectively. The PCL can be obtained by simply putting $\lambda = 0$ in equations (2.35), (S29) (top expression) and (S33) (top expression) for general thickness, and thin and semi-infinite limits respectively. All the limiting expressions for X are summarized in table S2. The compressibility limit expressions for θ are also presented in the last column for reference. Examining the expressions for X and θ for thin and semi-infinite cases of PCL and PIL, we infer that while incompressibility can be seen to impart near-rigidity to a thin substrate (since $X = -\dfrac{\gamma^2}{3}\left(\dfrac{\lambda_{\mathrm{C}}+2G}{G}\right)x^2$ is $\mathrm{O}(\gamma^2)$ smaller than 1), its effect on a semi-infinite substrate is much more ameliorated

Table S2: Expressions for X and θ in thickness and compressibility limits

	X			
	Thin ($\gamma \ll 1$)	**Thick** ($\gamma \sim 1$)	**Semi-Infinite** ($\gamma \gg 1$)	θ
PCL ($\nu = 0$)	1	equation (2.35)	$\left.\frac{2}{x}\right\|_{x\neq 0}, \left.-\frac{1}{4}\right\|_{x=0}$	$\frac{\delta\Pi}{2G}$
Normal	1	equation (2.35)	$\left.\frac{(\lambda+2G)^2}{2G(\lambda+G)x}\right\|_{x\neq 0}, \left.-\frac{\lambda^2+3\lambda G+2G^2}{2\lambda^2+9\lambda G+11G^2}\right\|_{x=0}$	$\frac{\delta\Pi}{\lambda+2G}$
PIL ($\nu = 0.5$)	$-\frac{\gamma^2}{3}\left(\frac{\lambda_C+2G}{G}\right)x^2$	equation (2.36) with $\Lambda = [\Lambda_i] = [1,4,2,4,8]$	$\left.\frac{(\lambda_c+2G)}{2Gx}\right\|_{x\neq 0}, \left.-\frac{1}{2}\right\|_{x=0}$	$\frac{\delta\Pi}{\lambda_c+2G}$

as the dimensional deflection l^* gets reduced to half for the same G or to three-fourth for the same E_{Y}. These factors gets exactly recovered only when the pressure and deflection are one-way coupled for the complete range of ν, which leads to the pressure being same for the two limiting cases being considered.

S5 Computational Scheme for TWC (Two-Way Coupling between pressure and deflection)

For TWC, the solution is obtained by numerically solving the discretized versions of the equations as listed out at the start of section 3. Note that we explicitly apply the boundary conditions,

$$\left.\frac{dl}{dr}\right|_{r=0} = 0, \qquad l|_{r\to\infty} \to 0, \tag{S35}$$

which has been obtained from equations (S16) and (S14). This is done as it generates smoother solution when dealing with relatively crude grid.

The multi-variable Newton-Raphson scheme is employed to solve the discretized equations, where the Hankel transformation kernel and the radial grid discretization are done in keeping with the discrete Hankel transformation formalism presented by Baddour & Chouinard (2015).

For equation (2.34), we use the discrete Hankel transformation formalism presented by Baddour & Chouinard (2015). Presented ahead is a concise version of their study that is pertinent to our problem. Their formalism utilizes the Fourier-Bessel series form of functions, according to which, any function $f(r)$ defined on a finite range $r = 0$ to $r = r_{\max}$ can be expanded in terms of a Fourier-Bessel series as,

$$f(r) = \sum_{\mathrm{k}=1}^{\infty} f_{\mathrm{k}} \mathcal{J}_{\mathrm{n}} \left(\frac{j_{\mathrm{n,k}} r}{r_{\max}} \right). \tag{S36}$$

In equation (S36), $\mathcal{J}$ represents Bessel function, n is the order of the Bessel function which is arbitrary, j_{nk} is the kth root of the Bessel function of order n, and f_{k} is the value of the function $f(r)$ at the point $r = r_k$ on the discretized grid, $r_{\mathrm{n,k}} = \dfrac{j_{\mathrm{n,k}} r_{\max}}{j_{\mathrm{n,N}}}$. Subsequent algebra yields the Hankel transformation kernel, Y as,

$$\mathrm{Y}^{\mathrm{n,N}}_{\mathrm{m,k}} = \frac{2}{j_{\mathrm{n,N}} \mathcal{J}^2_{\mathrm{n+1}}(j_{\mathrm{n,k}})} \mathcal{J}_{\mathrm{n}} \left(\frac{j_{\mathrm{n,m}} j_{\mathrm{n,m}}}{j_{\mathrm{n,N}}} \right) \qquad 1 \le \mathrm{m}, \qquad \mathrm{k} \le \mathrm{N\text{-}1} \tag{S37}$$

This transformation kernel is applicable for forward and inverse transformation between discretized functions $f(r)$ and its nth-order Hankel transform $\tilde{f}_{\mathrm{n}}(x)$, defined on the discretized grids, $r_{\mathrm{n,k}} = \dfrac{j_{\mathrm{n,k}} r_{\max}}{j_{\mathrm{n,N}}}$ and $x_{\mathrm{n,m}} = \dfrac{j_{\mathrm{n,m}}}{r_{\max}}$ respectively, each grid having N points. The forward transformation is defines as,

$$\tilde{f}_{\mathrm{n}}(x_{\mathrm{n,m}}) = \frac{r^2_{\max}}{j_{\mathrm{n,N}}} \sum_{\mathrm{k}=1}^{\mathrm{N\text{-}1}} \mathrm{Y}^{\mathrm{n,N}}_{\mathrm{m,k}} f(r_{\mathrm{n,k}}), \tag{S38}$$

and the inverse transform is defines as,

$$f(x_{\mathrm{n,k}}) = \frac{j_{\mathrm{n,N}}}{r^2_{\max}} \sum_{\mathrm{m}=1}^{\mathrm{N\text{-}1}} \mathrm{Y}^{\mathrm{n,N}}_{\mathrm{k,m}} \tilde{f}_{\mathrm{n}}(r_{\mathrm{n,m}}). \tag{S39}$$

Henceforth, we drop the superscripts n and N, with n being zero and N being implicitly considered.

Since the grid-sizes of discretized r and x are the same, N, we discretize equation (2.31) in real-space and equation (2.34) in Hankel space. Therefore, the discretized versions of these equations are,

$$\begin{aligned} & r_{\mathrm{k}}(H_{\mathrm{k}} + \Gamma l_{\mathrm{k}})^3 \left.\frac{d^2 p_{\mathrm{hd}}}{dr^2}\right|_{\mathrm{k}} + \\ & \left[(H_{\mathrm{k}} + \Gamma l_{\mathrm{k}})^3 + 3 r_{\mathrm{k}} (H_{\mathrm{k}} + \Gamma l_{\mathrm{k}})^2 \left(r_{\mathrm{k}} + \Gamma \left.\frac{dl}{dr}\right|_{\mathrm{k}} \right) \right] \left.\frac{dp_{\mathrm{hd}}}{dr}\right|_{\mathrm{k}} \\ & = 12 \frac{r_{\mathrm{k}} \theta}{\alpha \epsilon} \left[\left.\frac{dl}{dt}\right|_{\mathrm{k}} - \left(\frac{l_{\mathrm{k}}}{\theta} \frac{d\theta}{dt} + \frac{r_{\mathrm{k}}}{2k} \frac{dk}{dt} \left.\frac{\partial l}{\partial r}\right|_{\mathrm{k}} \right) \right] + 12 r_{\mathrm{k}} V_{\mathrm{S}}, \end{aligned} \tag{S40a}$$

$$\sum_{\mathrm{k=1}}^{\mathrm{N-1}} Y_{\mathrm{m,k}} \left(l_{\mathrm{k}} - X_{\mathrm{m}} p_{\mathrm{k}} \right) = 0. \tag{S40b}$$

The discretized equations (S40a) and (S40b) applies to the node points k=2 to k=N-1 and m=2 to m=N-1 respectively. At the centerline, i.e. k=1, the symmetric pressure and symmetric deflection boundary conditions apply, i.e.

$$\left. \frac{dp_{\mathrm{hd}}}{dr} \right|_{\mathrm{k}} = 0, \tag{S41a}$$

$$\left. \frac{dl}{dr} \right|_{\mathrm{k}} = 0. \tag{S41b}$$

At the far-end of the lubrication zone, i.e. k=N, the zero pressure and zero deflection boundary conditions apply, i.e.

$$p_{\mathrm{hd,k}} = 0, \tag{S42a}$$

$$l_{\mathrm{k}} = 0. \tag{S42b}$$

Equation (2.25) is simply approximated using trapezoidal rule for integration on the the discretized r-grid,

$$l_{\mathrm{S}} = 2\pi \sum_{\mathrm{k=1}}^{\mathrm{N-1}} (p_{\mathrm{k+1}} r_{\mathrm{k+1}} + p_{\mathrm{k}} r_{\mathrm{k}})(r_{\mathrm{k+1}} - r_{\mathrm{k}}) \tag{S43}$$

For each time instance, we solve equations (S40) to (S43) using the multivariable Newton-Raphson scheme (Press *et al.*, 1997). For this scheme, $p_{\mathrm{hd,k}}$, k=1 to k=N constitute the first N unknowns and l_{k}, k=1 to k=N constitute the next N unknowns, and l_{S} represents one unknown, totalling 2N+1 unknowns. Sub-equations a in equations (S40) to (S42) constitute the first N required equations, and subequations b constitute the next N required equations. The last equation is equation (S43), thus closing the system of equations.
The expressions for the residuals are,

$$\begin{aligned}
\mathrm{R_k} = {} & \left. \frac{dp_{\mathrm{hd}}}{dr} \right|_{\mathrm{k}} && \text{for k} = 1 \\
\mathrm{R_k} = {} & r_{\mathrm{k}} (H_{\mathrm{k}} + \Gamma l_{\mathrm{k}} + \Gamma_{\mathrm{S}} l_{\mathrm{S,k}})^3 \left. \frac{d^2 p_{\mathrm{hd}}}{dr^2} \right|_{\mathrm{k}} + \left. \frac{dp_{\mathrm{hd}}}{dr} \right|_{\mathrm{k}} \\
& \left[(H_{\mathrm{k}} + \Gamma l_{\mathrm{k}} + \Gamma_{\mathrm{S}} l_{\mathrm{S,k}})^3 + \right. \\
& \left. 3 r_{\mathrm{k}} (H_{\mathrm{k}} + \Gamma l_{\mathrm{k}} + \Gamma_{\mathrm{S}} l_{\mathrm{S,k}})^2 \left(r_{\mathrm{k}} + \Gamma \left. \frac{dl}{dr} \right|_{\mathrm{k}} \right) \right] \\
& - 12 r_{\mathrm{k}} V && \text{for k} = 2 \text{ to N} - 1 \\
\mathrm{R_k} = {} & p_{\mathrm{hd,k}} && \text{for k} = \mathrm{N} \\
\mathrm{R_k} = {} & \left. \frac{dl}{dr} \right|_{\mathrm{k}} && \text{for k} = 1 \\
\mathrm{R_{N+k}} = {} & \sum_{\mathrm{k=1}}^{\mathrm{N-1}} Y_{\mathrm{m,k}} \left(l_{\mathrm{k}} - X_{\mathrm{m}} p_{\mathrm{k}} \right) && \text{for k} = 2 \text{ to N} - 1 \\
\mathrm{R_{N+k}} = {} & l_{\mathrm{k}} && \text{for k} = \mathrm{N} \\
\mathrm{R_{2N+1}} = {} & \frac{l_{\mathrm{S}}}{\pi} - \sum_{\mathrm{k=1}}^{\mathrm{N-1}} (p_{\mathrm{k+1}} r_{\mathrm{k+1}} + p_{\mathrm{i}} r_{\mathrm{i}})(r_{\mathrm{k+1}} - r_{\mathrm{k}})
\end{aligned}$$

and the expressions for the Jacobians are,

$$
\begin{aligned}
\mathrm{J}_{\mathrm{k},\mathrm{k}+\kappa} &= \mathrm{a}_{\mathrm{k},\kappa}^{\mathrm{FD}(r)} && \text{for } \mathrm{k}=1, \kappa=0 \text{ to } 2\\
\mathrm{J}_{\mathrm{k},\mathrm{k}+\kappa} &= r_{\mathrm{k}}(H_{\mathrm{k}}+\Gamma l_{\mathrm{k}}+\Gamma_{\mathrm{S}} l_{\mathrm{S,k}})^3 \mathrm{a}_{\mathrm{k},\kappa}^{\mathrm{CD}(rr)} + \mathrm{a}_{\mathrm{k},\kappa}^{\mathrm{CD}(r)} \\
&\quad \left[(H_{\mathrm{k}}+\Gamma l_{\mathrm{k}}+\Gamma_{\mathrm{S}} l_{\mathrm{S,k}})^3 + \right. \\
&\quad \left. 3r_{\mathrm{k}}(H_{\mathrm{k}}+\Gamma l_{\mathrm{k}}+\Gamma_{\mathrm{S}} l_{\mathrm{S,k}})^2 \left(r_{\mathrm{k}}+\Gamma \left.\frac{dl}{dr}\right|_{\mathrm{k}}\right)\right] && \text{for } \mathrm{k}=2 \text{ to } \mathrm{N}-1, \kappa=-1 \text{ to } 1\\
\mathrm{J}_{\mathrm{k},\mathrm{N}+\mathrm{k}+\kappa} &= 3\Gamma \left[\left\{\left\{ r_{\mathrm{k}}(H_{\mathrm{k}}+\Gamma l_{\mathrm{k}}+\Gamma_{\mathrm{S}} l_{\mathrm{S,k}})^2 \left.\frac{d^2 p_{\mathrm{hd}}}{dr^2}\right|_{\mathrm{k}} + \right.\right.\right. \\
&\quad \left.\left.\left((H_{\mathrm{k}}+\Gamma l_{\mathrm{k}}+\Gamma_{\mathrm{S}} l_{\mathrm{S,k}})^2 + \right.\right.\right. \\
&\quad \left.\left.\left. 2r_{\mathrm{k}}(H_{\mathrm{k}}+\Gamma l_{\mathrm{k}}+\Gamma_{\mathrm{S}} l_{\mathrm{S,k}}) \left(r_{\mathrm{k}}+\Gamma \left.\frac{dl}{dr}\right|_{\mathrm{k}}\right)\right) \left.\frac{dp_{\mathrm{hd}}}{dr}\right|_{\mathrm{k}} - \right. \\
&\quad \left.\left. \frac{4r_{\mathrm{k}} k \mathrm{a}_{\mathrm{it},0}^{\mathrm{BD}(t)}}{\alpha} \right\} - \frac{4r_{\mathrm{k}} k}{\alpha\theta}\frac{d\theta}{dt} \right\} \mathrm{a}_{\mathrm{k},\kappa}^{\mathrm{CD}(0)} + \\
&\quad \left\{ r_{\mathrm{k}}(H_{\mathrm{k}}+\Gamma l_{\mathrm{k}}+\Gamma_{\mathrm{S}} l_{\mathrm{S,k}})^2 \left.\frac{dp_{\mathrm{hd}}}{dr}\right|_{\mathrm{k}} + \frac{2r_{\mathrm{k}}^2}{\alpha}\frac{dk}{dt} \right\} \mathrm{a}_{\mathrm{k},\kappa}^{\mathrm{CD}(r)} \Big] && \text{for } \mathrm{k}=2 \text{ to } \mathrm{N}-1, \kappa=-1 \text{ to } 1\\
\mathrm{J}_{\mathrm{k},2\mathrm{N}+1+\kappa} &= 3\Gamma_{\mathrm{S}} \left[\left\{ r_{\mathrm{k}}(H_{\mathrm{k}}+\Gamma l_{\mathrm{k}}+\Gamma_{\mathrm{S}} l_{\mathrm{S,k}})^2 \left.\frac{d^2 p_{\mathrm{hd}}}{dr^2}\right|_{\mathrm{k}} + \right.\right. \\
&\quad \left.\left.\left((H_{\mathrm{k}}+\Gamma l_{\mathrm{k}}+\Gamma_{\mathrm{S}} l_{\mathrm{S,k}})^2 + \right.\right.\right. \\
&\quad \left.\left.\left. 2r_{\mathrm{k}}(H_{\mathrm{k}}+\Gamma l_{\mathrm{k}}+\Gamma_{\mathrm{S}} l_{\mathrm{S,k}}) \left(r_{\mathrm{k}}+\Gamma \left.\frac{dl}{dr}\right|_{\mathrm{k}}\right)\right) \left.\frac{dp_{\mathrm{hd}}}{dr}\right|_{\mathrm{k}} - \right. \\
&\quad \left.\left. \frac{4r_{\mathrm{k}} k \mathrm{a}_{\mathrm{it},0}^{\mathrm{BD}(t)}}{\alpha} \right\} - \frac{4r_{\mathrm{k}} k}{\alpha\theta_{\mathrm{S}}}\frac{d\theta_{\mathrm{S}}}{dt} \right] && \text{for } \mathrm{k}=2 \text{ to } \mathrm{N}-1\\
\mathrm{J}_{\mathrm{k},\mathrm{k}} &= 1 && \text{for } \mathrm{k}=N\\
\mathrm{J}_{\mathrm{N}+\mathrm{k},\mathrm{N}+\mathrm{k}+\kappa} &= \mathrm{a}_{\mathrm{k},\kappa}^{\mathrm{FD}(r)} && \text{for } \mathrm{k}=1, \kappa=0 \text{ to } 2\\
\mathrm{J}_{\mathrm{N}+\mathrm{m},\mathrm{k}} &= -Y_{\mathrm{m,k}} X_{\mathrm{m}} && \text{for } \mathrm{m}=2 \text{ to } \mathrm{N}-1\\
\mathrm{J}_{\mathrm{N}+\mathrm{m},\mathrm{N}+\mathrm{k}} &= Y_{\mathrm{m,k}} \left(1 - X_{\mathrm{m}} \left.\frac{\mathcal{D}p_{\mathrm{nhd}}}{\mathcal{D}l}\right|_{\mathrm{k}}\right) && \text{for } \mathrm{m}=2 \text{ to } \mathrm{N}-1\\
\mathrm{J}_{\mathrm{N}+\mathrm{k},\mathrm{N}+\mathrm{k}} &= 1 && \text{for } \mathrm{k}=N\\
\mathrm{J}_{2\mathrm{N}+1,\mathrm{k}} &= -\frac{\pi\mu\omega\alpha}{k^2\epsilon\Pi} \cdot \begin{cases} r_{\mathrm{k}}(r_{\mathrm{k}+1}-r_{\mathrm{k}}) & \mathrm{k}=1, \\ r_{\mathrm{k}}(r_{\mathrm{k}+1}-r_{\mathrm{k}-1}) & \text{for } 1<\mathrm{k}<\text{N-1}, \\ r_{\mathrm{k}}(r_{\mathrm{k}}-r_{\mathrm{k}-1}) & \mathrm{k}=N, \end{cases} \\
\mathrm{J}_{2\mathrm{N}+1,\mathrm{k}} &= -\pi\frac{\mathcal{D}p_{\mathrm{nhd}}}{\mathcal{D}l} \cdot \begin{cases} r_{\mathrm{k}}(r_{\mathrm{k}+1}-r_{\mathrm{k}}) & \mathrm{k}=1, \\ r_{\mathrm{k}}(r_{\mathrm{k}+1}-r_{\mathrm{k}-1}) & \text{for } 1<\mathrm{k}<\text{N-1}, \\ r_{\mathrm{k}}(r_{\mathrm{k}}-r_{\mathrm{k}-1}) & \mathrm{k}=N, \end{cases} \\
\mathrm{J}_{2\mathrm{N}+1,2\mathrm{N}+1} &= 1
\end{aligned}
$$

In the expressions for J, terms like $\mathrm{a}_{\mathrm{k},\kappa}^{\mathrm{CD(r)}}$ stands for the co-efficients in the finite-difference approximations applied to different derivatives. For example, the r-derivative of an arbitrary dependent variable $\mathbb{Y}$ is,

$$\left.\frac{\partial \mathbb{Y}}{\partial r}\right|_{\mathrm{k}} = \sum_{\kappa=-2}^{\kappa=2} \mathrm{a}_{\mathrm{k},\kappa}^{\mathrm{CD}(r)} \mathbb{Y}_{\mathrm{k},\mathrm{k}+\kappa}. \tag{S44}$$

The superscript 'BD','CD' and 'FD' imply backward, central and forward differentiation. The term in bracket in the superscript implies the 'derivative with', i.e. 'r' implies first derivative with r, 'rr' implies second derivative with r, and 0 implies no derivative, i.e. $\mathrm{a}_{\mathrm{k},\kappa}^{\mathrm{CD}(0)}$ is 1 for $\kappa=0$ and 0 otherwise. Lastly, $\mathcal{D}$ denotes variational derivative, and $\frac{\mathcal{D}p_{\mathrm{nhd}}}{\mathcal{D}l}$ denotes the variational derivative of total non-hydrodynamic pressure with l, i.e. the sum of the variational

derivatives of each non-hydrodynamic pressure component with l,

$$\begin{aligned}
\frac{\mathcal{D}p_{\mathrm{DL}}}{\mathcal{D}l} &= -k\Gamma\epsilon KRp_{\mathrm{DL}} \\
\frac{\mathcal{D}p_{\mathrm{vdW}}}{\mathcal{D}l} &= -\frac{3\Gamma p_{\mathrm{vdW}}}{(H+\Gamma l)} \\
\frac{\mathcal{D}p}{\mathcal{D}l} &= \frac{2n_0k_{\mathrm{B}}T}{\Pi}\frac{\mathcal{D}p_{\mathrm{DL}}}{\mathcal{D}l} + \frac{A_{\mathrm{sfw}}}{6\pi k^3\epsilon^3R^3\Pi}\frac{\mathcal{D}p_{\mathrm{vdW}}}{\mathcal{D}l}
\end{aligned} \tag{S45}$$

The solution for p_{hd} and l is obtained by iterating over the equations,

$$\begin{aligned}
p_{\mathrm{hd,k}} &= p_{\mathrm{hd,k}} - \left(\mathrm{J}^{-1}\mathrm{R}\right)_{\mathrm{k}}, \\
l_{\mathrm{k}} &= l_{\mathrm{k}} - \left(\mathrm{J}^{-1}\mathrm{R}\right)_{\mathrm{N+k}}, \\
l_{\mathrm{S}} &= l_{\mathrm{S}} - \left(\mathrm{J}^{-1}\mathrm{R}\right)_{\mathrm{2N+1}},
\end{aligned} \tag{S46}$$

till $||\mathrm{R}|| = \max\left[|\mathrm{R_k}|\right]_{\mathrm{k=1...2N}}$ reduces below a threshold, taken as 10^{-5} in our computations.

S6 Recovering Storage and Loss Moduli from Force Response

The oscillatory loading of the sphere, in the absence of a spring, is given as,

$$H_{\mathrm{I}}^* = H^* = 1 + \frac{r^{*2}}{2R} + h_0\cos(\omega t^*), \tag{S47}$$

i.e. the transient part of the sphere's oscillation is,

$$h^* = h_0\cos(\omega t^*). \tag{S48}$$

For the case of small amplitude of oscillation, i.e. when $h_0 \ll D \implies \alpha \ll 1$, the time evolution of force between the sphere and the substrate is appreciably close to sinusoidal, and can therefore be expressed as,

$$F^* = F_0\cos(\omega t^* + \phi). \tag{S49}$$

Note that ϕ is the lag of force F^* in comparison to the oscillatory loading h^*. This lag is $\pi/2$ for the case of sufficiently low oscillation frequency, where deformation of the substrate and its temporal variation are both low enough for the substrate to be practically rigid and thus force response to be purely viscous.

Equations (S48) and (S49) can be expressed in complex notation as,

$$h^* = h_0\exp(\iota\omega t^*), \tag{S50}$$

$$F^* = \bar{F}_0\exp(\iota\omega t^*), \tag{S51}$$

where $\bar{F}_0$ is complex and captures the lag ϕ. Based on $\bar{F}_0$, storage modulus G' and loss modulus G'' are defined as (Leroy & Charlaix, 2011),

$$\bar{G} = G' + \iota G'' = \frac{\bar{F}_0}{h_0}. \tag{S52}$$

S7 Auxiliary Results and Discussions

In the interest of brevity in the main document, we present some additional results here. These results are arranged as follows. In section S7.1, we present the deflection characteristics occurring in OWC (one way coupling) for the limiting systems discussed in section S4. We restrict the solution to OWC (by taking high value of E_{Y}) in order to recover the different ratios of deflection as expected for the limiting cases. In section S7.2, we demonstrate the replication of pertinent results by Wang *et al.* (2017); Leroy & Charlaix (2011) computed using our framework. In section S7.3, we present some supplementary results corresponding to section 4.1.1. In section S7.4, we present some supplementary results corresponding to section 4.3.

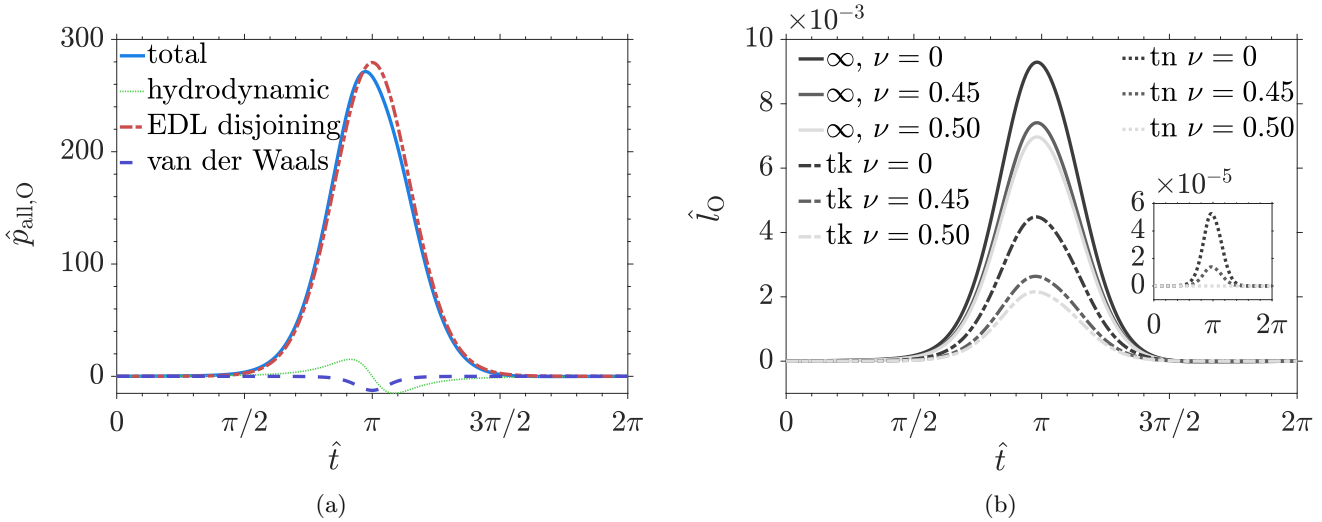

Figure S1: Variation of (a) normalized pressure components $\hat{p}_{\text{hd}}$, $\hat{p}_{\text{EDL}}$ and $\hat{p}_{\text{vdW}}$ and normalized net effective pressure $\hat{p}$ (labelled 'total'), and (b) normalized deflection $\hat{l}$ at origin, with normalized time $\hat{t}$ for oscillatory loading for demonstration of limiting cases discussed in section S4 and presented in table S2; system parameter values are: $R = 1$ mm, $D = 50$ nm, $h_0 = 45$ nm, $L = [0.5$ mm (semi-infinite, labelled '∞'), 5 μm (thick, labelled 'tk'), 50 nm (thin, labelled 'tn')], $\omega = 2\pi$ rad/s, $E_{\text{Y}} = 17.5$ GPa, $\nu = [0.00$ (PCL), 0.45 (normal), 0.50 (PIL)], $\mu = 1$ mPa-s, $A_{\text{sfw}} = 10^{-20}$ J, $\psi_0 = 2500$ mV.

S7.1 Limiting Cases

Here we present solutions corresponding to the limiting cases discussed in section S4 (each of the limiting cases presented table S2). We study oscillatory loading and choose a set of parameter values such that the pressure-deflection FSI coupling remains OWC for the entire oscillation. Since the coupling is one-way, the net effective pressure and individual pressure components exhibit time evolution (presented in figure S1a) which are identical for all the cases. Resulting time evolution of deflection for the different limiting cases is presented in figure S1b. For each limiting case, deflection plot obtained using the corresponding limiting expressions for X (as given in table S2) and using the complete expression for X coincide. The trends agree with expectations we set in section S4.

The deflection for thin substrate in PIL (perfectly incompressible limit) is nearly zero. The ratio of deflection for thin substrate, in PCL (perfectly compressible limit) to normal compressibility, is expected to be $\dfrac{X_{\text{thin,PCL}} \cdot \theta_{\text{PCL}}}{X_{\text{thin,normal}} \cdot \theta_{\text{normal}}} = \dfrac{1 \cdot \delta\Pi \cdot \frac{1}{2G_{\text{PCL}}}}{1 \cdot \delta\Pi \cdot \frac{1}{(\lambda+2G)_{\text{normal}}}} = \dfrac{\frac{1}{E_{\text{Y}}} \cdot (1+\nu_{\text{PCL}})}{\frac{1}{E_{\text{Y}}} \cdot \frac{(1+\nu_{\text{normal}})(1-2\nu_{\text{normal}})}{(1-\nu_{\text{normal}})}} = \dfrac{(1+0.0)}{\frac{(1+0.45)(1-2\cdot 0.45)}{(1-0.45)}} = 3.79$, which matches the ratio $\dfrac{\hat{l}_{\text{max,PCL}}}{\hat{l}_{\text{max,normal}}} = \dfrac{5.26}{1.38} = 3.79$. The ratio of deflection for semi-infinite substrate, in PCL to normal compressibility to PIL, is expected to be $[xX]_{\text{semi-infinite,PCL}} \cdot \theta_{\text{PCL}} : [xX]_{\text{semi-infinite,normal}} \cdot \theta_{\text{normal}} : [xX]_{\text{semi-infinite,PIL}} \cdot \theta_{\text{PIL}} = 2 \cdot \left[\dfrac{1}{2G}\right]_{\text{PCL}} \cdot \delta\Pi : \left[\dfrac{(\lambda+2G)^2}{2G(\lambda+G)} \cdot \dfrac{1}{(\lambda+2G)}\right]_{\text{normal}} \cdot \delta\Pi : \left[\dfrac{(\lambda_{\text{C}}+2G)}{2G} \cdot \dfrac{1}{(\lambda_{\text{C}}+2G)}\right]_{\text{PCL}} \cdot \delta\Pi = \left[\dfrac{1}{G}\right]_{\text{PCL}} : \left[\dfrac{(\lambda+2G)}{2G(\lambda+G)}\right]_{\text{normal}} : \left[\dfrac{1}{2G}\right]_{\text{PCL}} = \dfrac{2(1+\nu_{\text{PCL}})}{E_{\text{Y}}} : \dfrac{2(1-\nu_{\text{normal}})(1+\nu_{\text{normal}})}{E_{\text{Y}}} : \dfrac{(1+\nu_{\text{PIL}})}{E_{\text{Y}}} = 2(1+\nu_{\text{PCL}}) : 2(1-\nu_{\text{normal}})(1+\nu_{\text{normal}}) : (1+\nu_{\text{PIL}}) = 2(1+0.0) : 2(1-0.45)(1+0.45) : (1+0.5) = 2 : 1.6 : 1.5$, which matches with the ratio $\hat{l}_{\text{max,PCL}} : \hat{l}_{\text{max,normal}} : \hat{l}_{\text{max,PCL}} = 9.29 : 7.41 : 6.97 = 2 : 1.6 : 1.5$. Lastly, we highlight that such a comparison of ratios has been possible only because of OWC between deflection and pressure. In case of TWC (two way coupling), while the expectation of deflection being higher as substrate thickness and/or substrate material compressibility increases is qualitatively met, quantitative comparison is not possible. Hence, for the results discussed in the main document, which delves primarily into TWC regime, we have refrained from making a quantitative assessment of these limiting ratios.

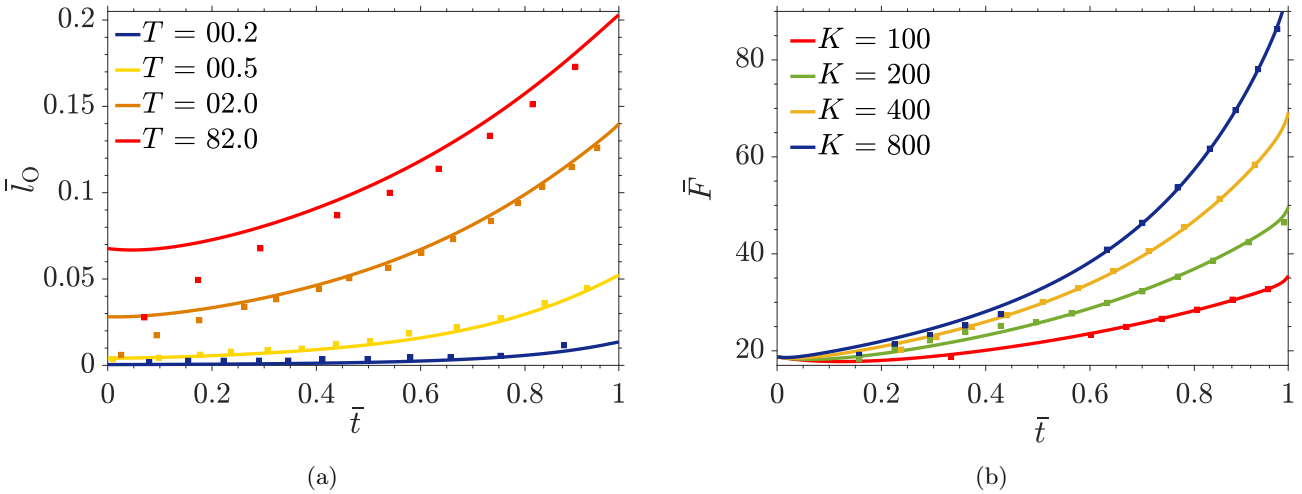

(a) (b)

Figure S2: Time evolution of (a) deflection for different substrate thicknesses, and (b) force for different spring constants; all variables are alternatively-normalized, as per non-dimensionalization scheme used by Wang *et al.* (2017); solid lines are computed solutions and square markers are values obtained by Wang *et al.* (2017).

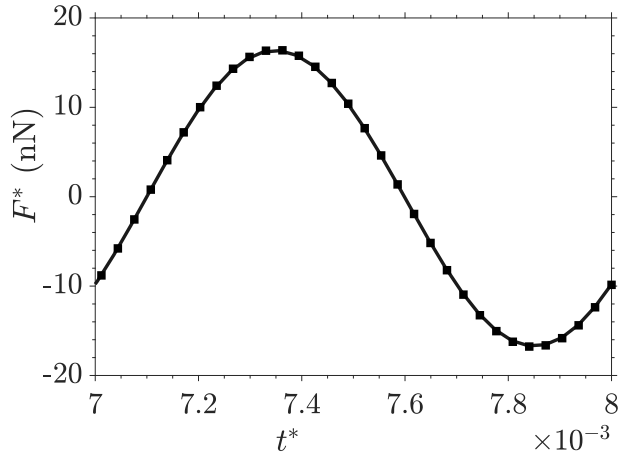

Figure S3: Quasi-steady variation with time t^* of Force F^* for high frequency low amplitude oscillations; system parameter values are: $R = 10$ μm, $D = 50$ nm, $h_0 = 1$ nm, $L = 1$ μm, $\hat{\omega} = 10^3$, $E_Y = 1.0$ MPa, $\nu = 0.45$, $\mu = 100$ mPa-s; square markers are computed values and solid line is sinusoidal curve obtained as per storage and loss modulus obtained by Leroy & Charlaix (2011).

S7.2 Replication of Results in Literature

As validation of our framework, we have computed some pertinent cases studied by Wang *et al.* (2017); Leroy & Charlaix (2011).

In figure S2, time evolution of deflection and force for some of the cases studied by Wang *et al.* (2017) is presented. The variables are 'alternatively-normalized', i.e. the computed dimensional solution is non-dimensionalized using the scheme employed by Wang *et al.* (2017) rather than using the normalization scheme outlined in table 2. The solid plot-lines are the computed results and the square markers are values obtained by Wang *et al.* (2017). Appreciable agreement can be observed between the two.

In figure S3, the quasi steady time evolution of force between sphere and substrate for a case of high-frequency low-amplitude oscillatory loading is presented. The input parameters match those for a case studied by Leroy & Charlaix (2011), and a sinusoidal force response is expected based on the storage and loss modulus given by them for this case. The computed solution is presented as the square markers and the expected sinusoidal force response is presented as the solid line. Appreciable match between the two can be observed.

S7.3 Supplementary Results for section 4.1.1

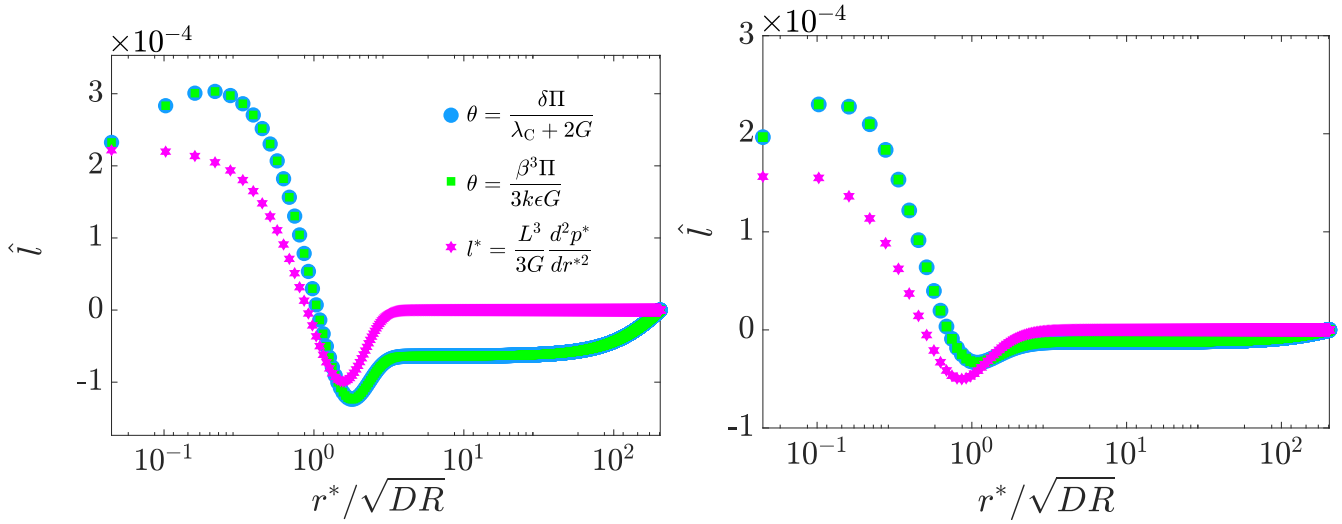

Figure S4: Radial variation of normalized deflection $\hat{l}$ at $t = 2$ for the thinnest incompressible substrate, i.e. $L = 93.81$ nm ($\hat{\beta} = 0.02$) and $\nu = 0.5$, corresponding to figure 2, panel (a) is without DLVO forces, and panel (b) is with DLVO force as per $\psi_0 = 100$ mV and $A_{\text{sfw}} = 10^{-21}$ J; other parameter values are the same as for figure 2; same legend applies to both panels.

Chandler & Vella (2020) present a combined foundation model for thin substrates, which accommodates both the Winkler foundation relation for the thin compressible substrate as well as a derived Laplacian of pressure relation (which gives $l^* = \frac{L^3}{3G}\frac{d^2p^*}{dr^{*2}}$) that exists for the thin incompressible limit. Based on the scaling principles in their study, the expression for θ for a thin incompressible substrate comes out as $\theta = \frac{\beta^3\Pi}{3k\epsilon G}$. However, as specified in the second last paragraph of section 2.6, any magnifying/diminishing effect of the work-around scaling $\left(\theta = \frac{\delta\Pi}{\lambda_C + 2G}\right)$ gets nullified due to a reciprocal scaling of X. For a thin incompressible substrate, this magnification/diminishing effect is stronger, but it gets nullified nonetheless. Hence, we do not need to necessarily alter the expression for θ (and X accordingly) even when we are dealing with a thin incompressible substrate. To verify that this indeed is the case, we have obtained the radial deflection profile at the end of sphere range of motion for two situations of approach loading for the thin incompressible substrate corresponding to figure 2, using the work-around scaling for θ, the scaling of θ as per Chandler & Vella (2020) (and X modified accordingly) and the Laplacian of pressure relation as given by Chandler & Vella (2020). These deflection profiles are depicted in figure S4. The deflection profile with the two scaling approaches are observably identical. They deviate from the Laplacian of prsessure relation to some extent, but exhibit appreciable similarity in trend. This deviation is probably a numerical artefact occurring because of the smallness of the deflection. Furthermore, it is to be noted that $\hat{l}$ is $O(10^{-4})$ indicating there is orders of magnitude smaller deflection of a thin substrate when its material is incompressible as opposed to compressible.

S7.4 Supplementary Results for section 4.3

The explicit time derivative terms on the right hand side of equation (2.31) imparts a transience to the system behaviour for high-frequency oscillations. This transience persists for larger number of oscillations for higher values of $\hat{\omega}$ and α, and hence, we have computed sufficient number of oscillations for each of the solutions corresponding to section 4.3. Here, we demonstrate one such solution in figure S5, where we show the time-evolution of force (top panel), the pressure at the origin (middle panel) and the deflection at the origin (bottom panel) for the case of $\hat{\omega} = 10^3$ with α and D as 0.1 and 10 nm. We can see that both pressure and deflection take about 15 oscillations to reach a quasi-steady state. In contrast, force $\hat{F}$ reaches a quasi-steady state in only two oscillations. We have observed that for the other cases also, the force reaches quasi-steady state faster than the pressure and the deflection.

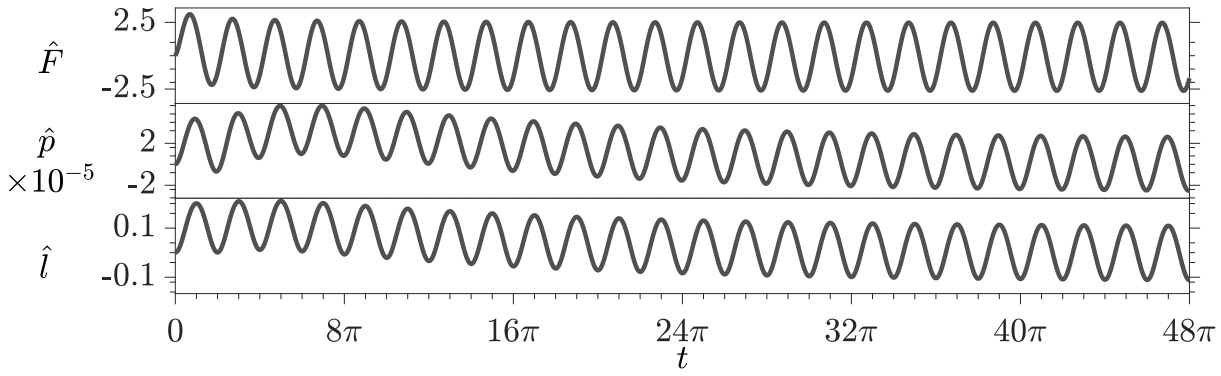

Figure S5: Variation of (top to bottom) force $\hat{F}$, pressure at origin $\hat{p}$ and deflection at origin $\hat{l}$ with time t for oscillatory loading with $D = 10$ nm, $\alpha = 0.1$, other parameter values are as in section 4.3.1.

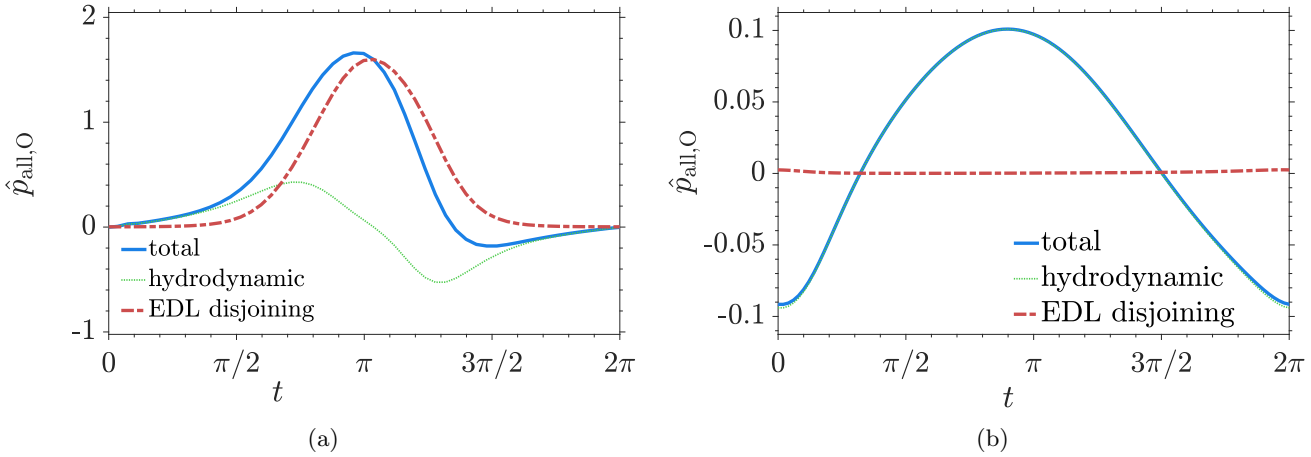

Figure S6: Quasi steady state variation of pressure components and net effective pressure at origin $\hat{p}_{\text{all(O)}}$ with time t for cases (ii) and (iv) discussed in section 4.3.1.

To demonstrate the contrast in the interplay of the underlying pressure components at different oscillation frequencies, in figure S6, we present the quasi-steady time evolution of pressure components and the net effective pressure for the cases of low frequency oscillations ($\hat{\omega} = 10^1$) and high frequency oscillations ($\hat{\omega} = 10^3$) with high oscillation amplitude ($\alpha = 0.7$) in the presence of van der Waals interactions, i.e cases (ii) and (iv) discussed in section 4.3.1. Amongst the DLVO pressure components, only the EDL disjoining pressure is appreciable in magnitude. It is sufficiently strong to dominate hydrodynamic pressure and therefore primarily dictates the net effective pressure and thus the force when the oscillation frequency is small (see figure S6a). However, since the hydrodynamic pressure grows in scale proportionately with the oscillation frequency, the net effective pressure is practically the same as the hydrodynamic pressure when the oscillation frequency is large (see figure S6b).

References

Ai, ZY, Yue, ZQ, Tham, LG & Yang, M 2002 Extended sneddon and muki solutions for multilayered elastic materials. *Int. J. Eng. Sci. (Oxford, U. K.)* **40** (13), 1453–1483.

Baddour, Natalie & Chouinard, Ugo 2015 Theory and operational rules for the discrete hankel transform. *J. Opt. Soc. Am.* **32** (4), 611–622.

Chan, KS, Karasudhi, P & Lee, SL 1974 Force at a point in the interior of a layered elastic half space. *Int. J. Solids Struct.* **10** (11), 1179–1199.

Chandler, Thomas GJ & Vella, Dominic 2020 Validity of winkler's mattress model for thin elastomeric layers: beyond poisson's ratio. *Proc. R. Soc. A* **476** (2242), 20200551.

Dhaliwal, Ranjit S & Rau, Indiresh S 1970 The axisymmetric boussinesq problem for a thick elastic layer under a punch of arbitrary profile. *Int. J. Eng. Sci. (Oxford, U. K.)* **8** (10), 843–856.

Gacoin, Eric, Frétigny, Christian, Chateauminois, Antoine, Perriot, A & Barthel, Etienne 2006 Measurement of the mechanical properties of thin films mechanically confined within contacts. *Tribol. Lett.* **21** (3), 245.

Giannakopoulos, AE & Suresh, S 1997 Indentation of solids with gradients in elastic properties: Part ii. axisymmetric indentors. *Int. J. Solids Struct.* **34** (19), 2393–2428.

Harding, JW & Sneddon, IN 1945 The elastic stresses produced by the indentation of the plane surface of a semi-infinite elastic solid by a rigid punch. *Math. Proc. Cambridge Philos. Soc.* **41** (1), 16–26.

Leal, L Gary 2007 *Advanced transport phenomena: fluid mechanics and convective transport processes*, , vol. 7. Cambridge University Press.

Leroy, S. & Charlaix, É 2011 Hydrodynamic interactions for the measurement of thin film elastic properties. *J. Fluid Mech.* **674**, 389–407.

Li, Jackie & Chou, Tsu-Wei 1997 Elastic field of a thin-film/substrate system under an axisymmetric loading. *Int. J. Solids Struct.* **34** (35-36), 4463–4478.

Muki, R 1960 Asymmetric problems of the theory of elasticity for a semi infinite solid and a thick plate. *Prog. Solid Mech.* pp. 399–439.

Press, William H, Teukolsky, Saul A, Vetterling, William T & Flannery, Brian P 1997 *Numerical Recipes in Fortran 77: The Art of Scientific Computing (Vol. I)*. Press Syndicate of the University of Cambridge.

Selvadurai, APS 2009 Boussinesq indentation of an isotropic elastic halfspace reinforced with an inextensible membrane. *Int. J. Eng. Sci. (Oxford, U. K.)* **47** (11-12), 1339–1345.

Selvadurai, APS & Lan, Q 1998 Axisymmetric mixed boundary value problems for an elastic halfspace with a periodic nonhomogeneity. *Int. J. Solids Struct.* **35** (15), 1813–1826.

Skotheim, J. M. & Mahadevan, L. 2004 Soft lubrication. *Phys. Rev. Lett.* **92** (24), 245509.

Urzay, J. 2010 Asymptotic theory of the elastohydrodynamic adhesion and gliding motion of a solid particle over soft and sticky substrates at low reynolds numbers. *J. Fluid Mech.* **653**, 391–429.

Wang, Yumo, Tan, Matthew R & Frechette, Joelle 2017 Elastic deformation of soft coatings due to lubrication forces. *Soft Matter* **13** (38), 6718–6729.

Yang, Fuqian 1998 Indentation of an incompressible elastic film. *Mech. Mater.* **30** (4), 275–286.

Yang, Fuqian 2003 Thickness effect on the indentation of an elastic layer. *Mater. Sci. Eng., A* **358** (1-2), 226–232.

Zhao, XJ & Rajapakse, RKND 2009 Analytical solutions for a surface-loaded isotropic elastic layer with surface energy effects. *Int. J. Eng. Sci. (Oxford, U. K.)* **47** (11-12), 1433–1444.